THE JOURNAL OF PHYSICAL CHEMISTRY A
A JOURNAL OF THE AMERICAN CHEMICAL SOCIETY

pubs.acs.org/JPCA

Article

Femtosecond 2 + 1 Resonance-Enhanced Multiphoton Ionization Spectroscopy of the *C*-State in Molecular Oxygen

Published as part of The Journal of Physical Chemistry virtual special issue "Daniel Neumark Festschrift".

Ana Caballo, Anders J.T.M. Huits, Arno Vredenborg, Michiel Balster, David H. Parker, and Daniel A. Horke*

Cite This: *J. Phys. Chem. A* 2021, 125, 9060−9064

Read Online

ACCESS | Metrics & More | Article Recommendations

ABSTRACT: Coincidence electron-cation imaging is used to characterize the multiphoton ionization of O_2 via the v = 4,5 levels of the 3s($^3\Pi_g$) Rydberg state. A tunable 100 fs laser beam operating in the 271−263 nm region is found to cause a nonresonant ionization across this wavelength range, with an additional resonant ionization channel only observed when tuned to the $^3\Pi_g(v = 5)$ level. A distinct 3s → p wave character is observed in the photoelectron angular distribution for the v = 5 channel when on resonance.

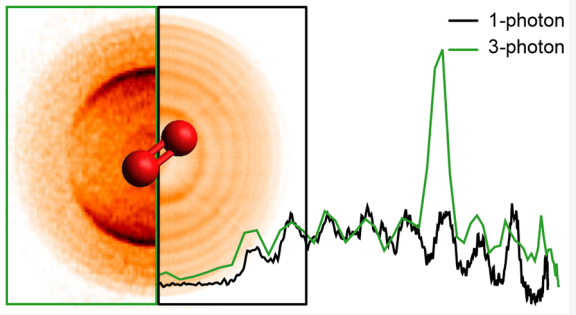

I. INTRODUCTION

After decades of intensive study, the energy positions, absorption cross sections, and symmetry assignments of most of the one- and two-photon observable excited electronic states of molecular oxygen are now reasonably certain.[1,2] Since almost all of the numerous excited states of O_2 dissociate directly or indirectly after an absorption,[3,4] each molecular quantum level (electronic, vibrational, and rotational) can show state-dependent lifetimes and follow specific multiple pathways to the six possible valence dissociation limits that are paired combinations of O(^{3}P), O(^{1}D), and O(^{1}S) fragment atoms.[5] A particularly powerful method for tracing out the optically forbidden ro-vibronic states of O_2 is to scan the photon energy while detecting ions from two-photon resonant, one-photon ionization (2 + 1 REMPI), illustrated schematically in Figure 1 for the energy region of this study.

Normally, in a resonance-enhanced multiphoton ionization (REMPI) study, where $O_2 + 3h\nu \rightarrow O_2^+ + e^-$, it makes most sense to mass-selectively detect the O_2^+ ion. However, a detection of the partner electron can provide additional and readily accessible information on the resonant excited state, which we take advantage of in this work. One disadvantage arising from the detection of electrons is that the intense, short-duration UV laser pulses necessary for this study create electrons from metal surfaces and from any other molecule present in the apparatus. This makes electron detection significantly more challenging, in particular, for weak transitions and for wavelengths within the absorption range of water and other common contaminants. We show here that

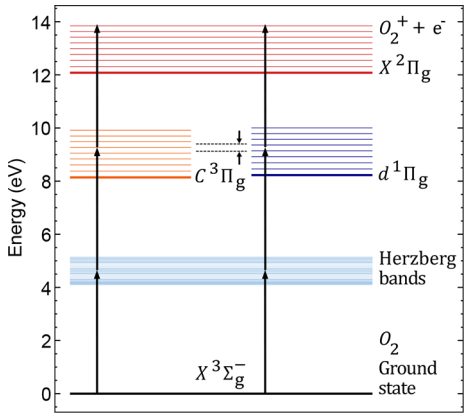

Figure 1. Schematic energy level diagram for the electronic and vibrational levels of O_2 and O_2^+ states at the one-, two-, and three-photon energy used in this study. At the two-photon level the $C^3\Pi_g$ state is spin-allowed, but spin−orbit coupling allows an excitation also to the spin-forbidden $d^1\Pi_g$ state. The energy range with two-photon excitation covered in this study is indicated by up−down arrows.

Received: June 23, 2021
Revised: September 8, 2021
Published: October 11, 2021

https://doi.org/10.1021/acs.jpca.1c05541
J. Phys. Chem. A 2021, 125, 9060−9064

electron-cation coincidence imaging detection[6,7] successfully extracts the $O_2 + 3h\nu \rightarrow O_2^+ + e^-$ process from a significant background, revealing a low-resolution but still informative REMPI spectrum.

Our goal is to trace out the $v = 4$ and 5 vibrational levels of the $3s(^3\Pi_g, {}^1\Pi_g)$ states, which are the lowest-lying and most intensively studied Rydberg states of O_2. The spin−orbit mixing of the $C^3\Pi_g$ and $d^1\Pi_g$ states is significant,[2] making the spin-forbidden d-states observable, especially with nanosecond laser excitation, where the competition of ionization with predissociation favors the detection of longer-lived intermediate states. Because of the rapid predissociation and extremely low Franck−Condon factors for these target states, an intense and tunable laser beam is necessary. Previous work in this wavelength range was performed by Conde et al.,[8] who studied the two-photon excitation of O_2 in the 304−220 nm region, with a time-delayed 800 nm ionization to detect remaining O_2^+ ions. They reported O_2^+ decay lifetimes for the $3s^3\Pi_g$ ($v = 0-3$) states, assuming that their 35 fs pulse duration laser ionizes all levels in the C, d manifold with equal efficiency (measured lifetimes ranged from 24 to 812 fs), so that primarily the spin-allowed C states are excited.

For typical femtosecond REMPI studies,[9,10] the laser bandwidth is broader than the ro-vibrational envelopes studied, making a spectral assignment of the actual excitation with cation detection impossible. However, the image of electrons created by the ionization step can provide key additional information.[11] We utilized here a pulse-amplified 100 fs duration Ti-sapphire laser, where the fundamental wavelength was tunable in the range of 790−815 nm, corresponding to a tuning range of the third harmonic of 263−271 nm, as indicated in Figure 1. The three-photon ionization at these wavelengths leads to the creation of $O_2^+ X^2\Pi_g$ ($v = 0-8$) + e^-, with the ionic vibrational spacing of ∼0.22 eV. Since most, but not all, of the excess energy goes into the kinetic energy of the electron, the electron image can show up to nine rings covering the range of 0−1.8 eV. For cation detection, momentum conservation yields an ∼0.25 μeV vibrational spacing ($v = 0-1$) in the recoiling O_2^+ partner, which is not resolvable. The recorded electron image therefore yields significant additional information, not only speed and thus which vibrational state of the ion is formed but also angular information on the orbital character of the ionized electron. In particular, we find a strong enhancement via the $C^3\Pi_g$ ($v = 5$) at 267.33 nm, while no resonance with the $d^1\Pi_g$ state was observed within the wavelength range covered here. Although sharp discrete transitions to the Herzberg states are present in the one-photon region of this study, these are very weak and are found not to cause a resonance enhancement of the measured signal.

II. METHODS

Data were collected using a photoelectron-photoion coincidence imaging spectrometer, coupled to a femtosecond laser system. The setup has previously been described in detail, and only the main features pertinent to the current experiment are outlined here.[7] The vacuum system consisted of three differentially pumped chambers, separated by molecular beam skimmers placed 2 cm (500 μm diameter) and 14 cm (200 μm diameter) after the source. The continuous molecular beam was produced in a conical nozzle with a ∼40 μm pinhole, with a typical O_2 pressure of 1.5 bar. The base pressure in the detection chamber was on the order of 10^{-10} mbar. Here the molecular beam was crossed by femtosecond laser pulses in the center of a double-sided velocity-map imaging (VMI) spectrometer,[12] equipped with two time- and position-sensitive detectors (DLD40X, RoentDek). Extraction fields in the VMI were switched from electron to ion extraction to ensure optimal imaging conditions for both.

The commercial laser system consisted of a titanium-sapphire oscillator and a regenerative amplifier (Spectra Physics *Spitfire Ace*), operated at a 3 kHz repetition rate with typical pulse durations of 100 fs. The central wavelength can be tuned in the range from ∼790 to 815 nm. Pulses in the UV were produced by a subsequent frequency doubling and tripling in β-barium borate (BBO) crystals, yielding pulses in the range of 263−271 nm with a typical bandwidth (full width at half-maximum (fwhm)) of 3 nm. The pulse duration was estimated to be 170 fs fwhm from the measured cross-correlation of a 266 nm pulse with an additional 400 nm one inside the detection chamber. The UV output was attenuated to ∼15 μJ, and it was focused into the interaction region with an f = 500 mm lens. This power density corresponds to a Keldysh parameter of ∼26 for O_2, well within the multiphoton ionization regime. The polarization was kept parallel to the imaging detectors.

Data were collected by use of the CoboldPC software (RoentDek), and only events containing a single electron hit in coincidence with a single ion hit were kept for further analysis. Photoelectron images of interest were extracted by only considering electrons detected in coincidence with an O_2^+ ion. Images were Abel-inverted using the basis set expansion method (basex), as implemented in the PyAbel Python package,[13] calibrated to the well-known vibrational levels of oxygen and normalized with respect to the total measurement time.

III. RESULTS AND DISCUSSION

Photoelectron images were collected for five distinct wavelengths in the region of 263−271 nm, leading to an ionization of O_2 in a three-photon process. The corresponding photoelectron spectra (PES) and two representative photoelectron images are shown in Figure 2. All PES show a clear vibrational structure, which we assign to the ground state of the produced O_2^+ ion ($X^2\Pi_g$). For the shortest wavelengths employed, vibrational levels up to $v = 8$ are accessible, consistent with the known energetics (see the three-photon energy and ion states shown in Figure 1).

With the exception of the PES collected at 267.33 nm, all spectra exhibit a nearly uniform intensity distribution across the observed O_2^+ ion vibrational levels. This is indicative of a nonresonant three-photon ionization, as might be expected for the ultrafast pulses used in the experiment. The vibrational distributions should in this case reflect the Franck−Condon factor between the neutral ground state $X^3\Sigma_g^-$ and the ion ground state $X^2\Pi_g$. Nonetheless, similar intensities are observed for ion vibrational levels $v = 0-8$. This behavior could be due to the presence of an autoionizing valence state in the three-photon energy region, which has been previously reported in a study of the $C^3\Pi_g$ ($v = 2$) state.[14] Tuning the wavelength to 267.33 nm, however, leads to a steep increase in photoelectrons at kinetic energies associated with the $v = 5$ level of the ion. This is very evident also in the presented photoelectron images in Figure 2, which are each normalized to the collection time and plotted on the same color scale.

We attribute this increased photoelectron signal to a resonance enhancement through an intermediate state reached

https://doi.org/10.1021/acs.jpca.1c05541
J. Phys. Chem. A 2021, 125, 9060−9064

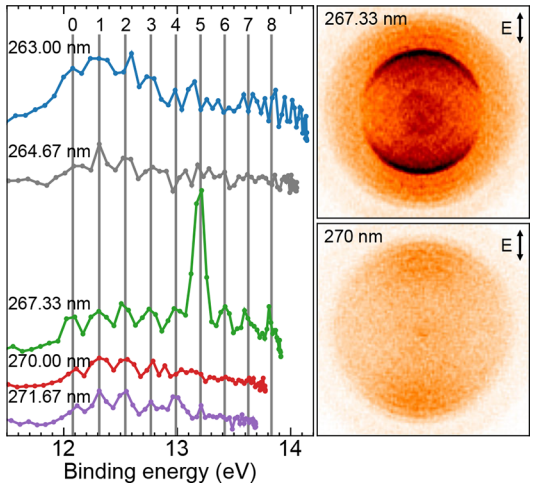

Figure 2. Photoelectron spectra for each excitation wavelength. The energies of the ion $X^2\Pi_g$ vibrational levels (v = 0−8) are shown with vertical lines. The right figures show the symmetrized raw photoelectron images for two wavelengths: resonant with the $C^3\Pi_g$ (v = 5) state (top) and nonresonant (bottom). The laser polarization is vertical in the image and indicated by a double-headed arrow.

via a two-photon transition, such that we are now observing a 2 + 1 REMPI process. To confirm the assignment of a two-photon resonance we compare our PES collected through a three-photon process at 267.33 nm to the corresponding single-photon spectrum collected at 89.5 nm (13.85 eV), as shown in Figure 3. This was collected using the DELICIOUS3

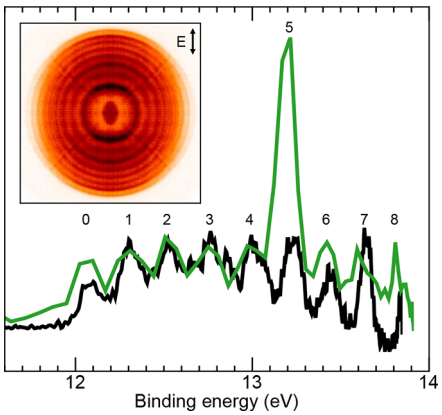

Figure 3. Photoelectron spectra measured in a three-photon (green trace) and one-photon (black trace) ionization process. The intensities are scaled such that the uniform one-photon distribution maxima match the intensity of the nonresonant features at the three-photon ionization. The ion $X^2\Pi_g$ vibrational levels (v = 0−8) are labeled. (inset) Symmetrized raw photoelectron image resulting from a one-photon excitation. The synchrotron radiation polarization is vertical in the image and indicated by a double-headed arrow.

coincidence spectrometer of the DESIRS beamline at the SOLEIL synchrotron source.[15,16] The single-photon spectrum shows an intensity distribution across the vibrational features that is approximately uniform, similar to the nonresonance three-photon spectra shown in Figure 2, and confirms our assignment of a two-photon resonance at 267.33 nm.

Further evidence of a resonant process occurring at 267.33 nm is available from the recorded photoelectron angular distributions (PADs), which were analyzed for each excitation wavelength and ion vibrational level. For the nonresonant wavelengths, they show a general trend of positive anisotropy with β_2 parameters in the range of ∼0.5−1.0 at v = 0−4 and decreasing toward higher vibrational levels, which are nearly isotropic. The extracted β_2 parameters for the resonance excitation at 267.33 nm are shown in Figure 4. While they

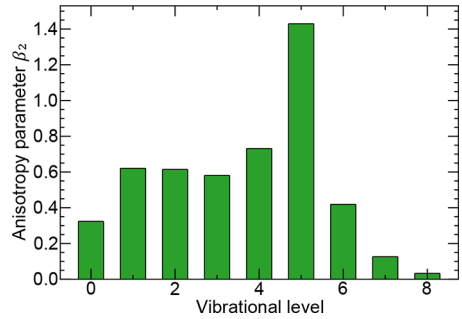

Figure 4. Anisotropy parameter β_2 extracted from the photoelectron image measured at 267.33 nm as a function of the ion $X^2\Pi_g$ vibrational level excited (v = 0−8).

exhibit the same trend as the other excitation wavelengths for vibrational ion states $v \neq 5$, a markedly larger aniosotropy is observed for v = 5, again confirming the contribtion of an additional channel. This is consistent with previously reported photoelectron angular distributions for the $C^3\Pi_g$ and $d^1\Pi_g$ states,[17,18] which showed a large positive beta for Δv = 0, consistent with an ejection of a (3)s electron into the p-wave continuum. PADs with $\Delta v \neq 0$ were found to be less anisotropic, reflecting increasing effects of autoionization and/or a shape resonance.[14]

To identify the resonant state, Figure 5 shows the employed two-photon energies and the relevant O_2 states in this energy range. At 267.33 nm, the two-photon energy matches that of the $C^3\Pi_g$ (v = 5) vibrational state, suggesting this resonance as the process behind the enhancement experimentally observed. If the $d^1\Pi_g$ (v = 5) level was also contributing to the resonance

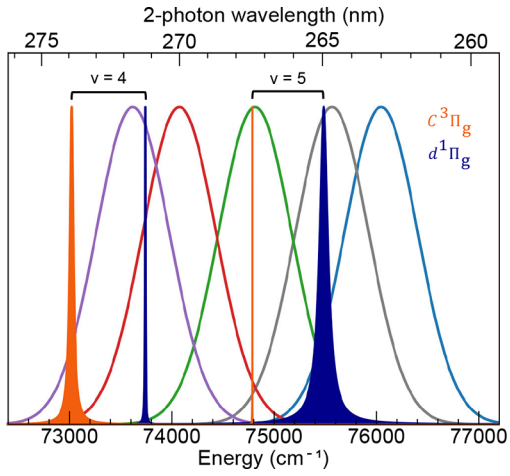

Figure 5. Energy diagram of the relevant Rydberg states along with the two-photon excitation energies used. The $C^3\Pi_g$ and $d^1\Pi_g$ (v = 4 and v = 5) states are represented by orange and dark blue curves. Their position and width correspond to available theoretical calculations.[2] The five colored gaussians indicate the two-photon excitation energies for the wavelengths scanned, with an fwhm that corresponds to the experimentally measured value.

https://doi.org/10.1021/acs.jpca.1c05541
J. Phys. Chem. A 2021, 125, 9060−9064

behavior, one would expect to see a strong resonance enhancement at 264.67 nm, which is not present in our measurements. This suggests that the $C^3\Pi_g \leftarrow X^3\Sigma_g^-$ transition is much stronger than the spin-forbidden $d^1\Pi_g \leftarrow X^3\Sigma_g^-$. Additionally, the tail of the laser bandwidth for the longest wavelength employed (271.67 nm) shows an overlap with the $C^3\Pi_g$ ($v = 4$) state. However, no enhancement of the ion $v = 4$ level is detected. Although the difference in overlap with the laser pulse complicates the comparison, this might imply that the $C^3\Pi_g$ state absorption is more sensitive to the strong and sharp $v = 5$ than it is to the $v = 4$, suggesting that only a small fraction of the excitation pulse is used in the REMPI process and highlighting the importance of the resonance enhancement.

IV. CONCLUSION AND OUTLOOK

Coincidence electron-cation imaging is shown here to reveal a two-photon resonance enhancement channel in the three-photon ionization of molecular oxygen by a femtosecond laser. Although the large laser bandwidth does not allow a full spectroscopic characterization of the resonance state, enhancement occurs only when the laser wavelength is tuned near 266.7 nm, which is consistent with the two-photon energy position of the $C^3\Pi_g$ ($v = 5$) state. Two-color pump−probe experiments, similar to those of Conde et al. for the $C^3\Pi_g$($v = 0-3$) states, are in progress to record the lifetime of the $C^3\Pi_g$ ($v = 5$) state for comparison with predictions by theory.[2] The use of ultrafast laser pulses with a ∼100 fs duration offers a good compromise between the spectral resolution for a selective REMPI process in small molecules and the time resolution to capture many dynamic processes. The extra information provided by electron imaging should be useful in any ultrafast pump−probe photodissociation dynamics study.

AUTHOR INFORMATION

Corresponding Author

Daniel A. Horke − *Institute for Molecules and Materials, Radboud University, 6525 AJ Nijmegen, The Netherlands;* orcid.org/0000-0002-9862-8108; Email: d.horke@science.ru.nl

Authors

Ana Caballo − *Institute for Molecules and Materials, Radboud University, 6525 AJ Nijmegen, The Netherlands*

Anders J.T.M. Huits − *Institute for Molecules and Materials, Radboud University, 6525 AJ Nijmegen, The Netherlands*

Arno Vredenborg − *Institute for Molecules and Materials, Radboud University, 6525 AJ Nijmegen, The Netherlands*

Michiel Balster − *Institute for Molecules and Materials, Radboud University, 6525 AJ Nijmegen, The Netherlands*

David H. Parker − *Institute for Molecules and Materials, Radboud University, 6525 AJ Nijmegen, The Netherlands;* orcid.org/0000-0003-0297-168X

Complete contact information is available at: https://pubs.acs.org/10.1021/acs.jpca.1c05541

Notes

The authors declare no competing financial interest.

ACKNOWLEDGMENTS

This work was supported by The Netherlands Organization for Scientific Research, under Grant No. STU.019.009, as well as the Spectroscopy of Cold Molecules Department and the Institute for Molecules and Materials of Radboud University Nijmegen. We thank the staff of SOLEIL, and, in particular, L. Nahon and G. Garcia, for the smooth running of the facility and for providing beamtime and expert experimental assisstance for Project 20150031. We thank Prof. B. van de Meerakker for many fruitful discussions and his continued enthusiasm and support for molecular physics research in Nijmegen.

REFERENCES

(1) Krupenie, P. H. The Spectrum of Molecular Oxygen. *J. Phys. Chem. Ref. Data* **1972**, *1*, 423−534.

(2) Morrill, J. S.; Ginter, M. L.; Lewis, B. R.; Gibson, S. T. The (X $^2\Pi_g$) nsσ_g $^{1,3}\Pi_g$ Rydberg States of O_2: Spectra, Structures, and Interactions. *J. Chem. Phys.* **1999**, *111*, 173−185.

(3) Leahy, J.; Cyr, R.; Osborn, L.; Neumark, D. M. Observation of the Correlated O^3P_{j1}, $^3P_{j2}$ State Distribution from the Predissociation of O_2 $B^3\Sigma_u^-$. *Chem. Phys. Lett.* **1993**, *216*, 503.

(4) Leahy, D. J.; Osborn, D. L.; Cyr, D. R.; Neumark, D. M. Predissociation Dynamics of the the O_2 $B^3\Sigma_u^-$ State: Vibrational State Dependence of the Product Fine-structure Distribution. *J. Chem. Phys.* **1995**, *103*, 2495−2508.

(5) Parker, D. H. Laser Photochemistry of Molecular Oxygen. *Acc. Chem. Res.* **2000**, *33*, 563−571.

(6) Vredenborg, A.; Lehmann, C. S.; Irimia, D.; Roeterdink, W. G.; Janssen, M. H. M. The Reaction Microscope: Imaging and Pulse Shaping Control in Photodynamics. *ChemPhysChem* **2011**, *12*, 1459−1473.

(7) Vredenborg, A.; Roeterdink, W. G.; Janssen, M. H. M. A photoelectron-photoion coincidence imaging apparatus for femtosecond time-resolved molecular dynamics with electron time-of-flight resolution of σ = 18ps and energy resolution ΔE/E = 3.5%. *Rev. Sci. Instrum.* **2008**, *79*, 063108.

(8) Conde, A. P.; Montero, R.; Ovejas, V.; Fernández-Fernández, M.; Castaño, F.; Longarte, A. Ultrafast Dynamics of the ns (n = 3,4) and 3d Rydberg States of O_2. *Phys. Chem. Chem. Phys.* **2013**, *15*, 4914.

(9) Baumert, T.; Bühler, B.; Thalweiser, R.; Gerber, G. Femtosecond Spectroscopy of Molecular Autoionization and Fragmentation. *Phys. Rev. Lett.* **1990**, *64*, 733−736.

(10) Murillo-Sánchez, M. L.; González-Vázquez, J.; Corrales, M. E.; de Nalda, R.; Martínez-Núñez, E.; García-Vela, A.; Bañares, L. Femtochemistry under Scrutiny: Clocking State-Resolved Channels in the Photodissociation of CH_3I in the *A* -Band. *J. Chem. Phys.* **2020**, *152*, 014304.

(11) Stolow, A.; Bragg, A. E.; Neumark, D. M. Femtosecond Time-Resolved Photoelectron Spectroscopy. *Chem. Rev.* **2004**, *104*, 1719−1758.

(12) Eppink, A. T. J. B.; Parker, D. H. Velocity map imaging of ions and electrons using electrostatic lenses: Application in photoelectron and photofragment ion imaging of molecular oxygen. *Rev. Sci. Instrum.* **1997**, *68*, 3477−3484.

(13) Hickstein, D. D.; Gibson, S. T.; Yurchak, R.; Das, D. D.; Ryazanov, M. A Direct Comparison of High-Speed Methods for the Numerical Abel Transform. *Rev. Sci. Instrum.* **2019**, *90*, 065115.

(14) Miller, P. J.; Li, L.; Chupka, W. A.; Colson, S. D. Shape Resonance and Non-Franck−Condon Behavior in the Photoelectron Spectra of O_2 produced by (2 + 1) Multiphoton Ionization via 3sσ Rydberg States. *J. Chem. Phys.* **1988**, *89*, 3921−3922.

(15) Nahon, L.; de Oliveira, N.; Garcia, G. A.; Gil, J.-F.; Pilette, B.; Marcouillé, O.; Lagarde, B.; Polack, F. DESIRS: A State-of-the-Art VUV Beamline Featuring High Resolution and Variable Polarization for Spectroscopy and Dichroism at SOLEIL. *J. Synchrotron Radiat.* **2012**, *19*, 508−520.

(16) Garcia, G. A.; Cunha de Miranda, B. K.; Tia, M.; Daly, S.; Nahon, L. DELICIOUS III: A Multipurpose Double Imaging Particle Coincidence Spectrometer for Gas Phase Vacuum Ultraviolet Photodynamics Studies. *Rev. Sci. Instrum.* **2013**, *84*, 053112.

(17) Katsumata, S.; Sato, K.; Achiba, Y.; Kimura, K. Excited-State Photoelectron Spectra of the One-Photon Forbidden $C^3\Pi_g$ Rydberg State of Molecular Oxygen. *J. Electron Spectrosc. Relat. Phenom.* **1986**, *41*, 325−335.
(18) Sur, A.; Ramana, C. V.; Chupka, W. A.; Colson, S. D. Rydberg−Valence Interactions in the Π_g states of O_2. *J. Chem. Phys.* **1986**, *84*, 69−72.

https://doi.org/10.1021/acs.jpca.1c05541
J. Phys. Chem. A 2021, 125, 9060−9064